Available online at www.sciencedirect.com
SCIENCE DIRECT®
Optics Communications 242 (2004) 345–350
OPTICS COMMUNICATIONS
www.elsevier.com/locate/optcom

Frequency domain phase-resolved optical Doppler and Doppler variance tomography

Lei Wang [a,c], Yimin Wang [b,d], Shuguang Guo [b,d], Jun Zhang [b,d], Mark Bachman [a,b,c], G.P. Li [a,b,c], Zhongping Chen [a,b,d,*]

[a] *Department of Electrical Engineering and Computer Science, University of California, Irvine, 1002 Health Science Road, Irvine, CA 92612 , USA*
[b] *Department of Biomedical Engineering, University of California, Irvine, CA, USA*
[c] *UCI Integrated Nanosystems Research Facility, University of California, Irvine, CA, USA*
[d] *Beckman Laser Institute, University of California, Irvine, CA, USA*

Received 3 December 2003; received in revised form 11 August 2004; accepted 19 August 2004

Abstract

Frequency domain phase-resolved optical Doppler tomography (ODT) was developed with Doppler variance imaging capability. It is shown that utilizing the frequency domain method, phase-resolved ODT can achieve much higher imaging speed and velocity dynamic range than the time domain method. Structural, Doppler and Doppler variance images of fluid flow through glass channels were quantified and blood flow through vessels were demonstrated in vivo.

Keywords: Optical Doppler tomography; Flowmetry

Optical Doppler tomography (ODT), also named Doppler optical coherence tomography (Doppler OCT), is capable of measuring microflows using the optical Doppler effect [1,2]. Early ODT systems were unable to achieve high imaging speed, high velocity sensitivity and high spatial resolution simultaneously. A phase-resolved algorithm was developed to obtain high velocity sensitivity while maintaining high imaging speed and high spatial resolution. This technique has been applied to clinical investigations [2,3] and microfluidic study [4]. To further the study of microflows, a Doppler variance algorithm has been added to the phase-resolved ODT [5]. Doppler frequency shift depends on the Doppler angle between the probe and the flow direction. By contrast, Doppler variance is less sensitive to Doppler angle and is more efficient for mapping the flows

* Corresponding author. Tel.: +1 9498241247; fax: +1 9498248413.
E-mail address: zchen@laser.bli.uci.edu (Z. Chen).

0030-4018/$ - see front matter
doi:10.1016/j.optcom.2004.08.035

buried in non-transparent media. Currently, ODT systems are implemented in the time domain. Although real-time 2D flow imaging has been achieved with the time domain ODT, 3D mapping of complex flows in microfluidic networks requires even higher speed and better sensitivity. In the time domain ODT, mechanical devices are required for axial scanning (A-line scanning) and limit the imaging speed and velocity dynamic range.

Recently, the frequency domain OCT has shown advantages in imaging speed and signal-to-noise ratio over the time domain OCT [6–13]. Since the velocity dynamic range of a phase-resolved ODT system is determined by A-line scanning rate, it would be advantageous to extract Doppler information using the frequency domain method. The measurement of flow profiles was demonstrated using frequency domain method [14,15], but the Doppler variance tomography has not been performed in frequency domain. In this paper, we demonstrate a frequency domain Doppler tomography system with Doppler variance imaging capability using phase-resolved algorithm to measure fluid flows through glass channels and blood vessels.

The schematic of the frequency domain ODT system is shown in Fig. 1. Low-coherence light generated by amplified spontaneous emission of a diode is coupled into the source arm of a fiber-based Michelson interferometer. Back-reflected light from the reference and sample arms are guided into a spectrometer. The dispersed spectrum is sampled by a photon detector array. With an object placed in the sample arm and with two optical paths matched, an interference pattern will be generated on the detector array. The frequency domain representation of the interference pattern is described by [7]

$$F(k) = S(k)\left[1 + \int_0^\infty \int_0^\infty a(z)a(z') \times \exp\left[-2kn(z-z')\right] \mathrm{d}z\, \mathrm{d}z' + 2\int_0^\infty a(z)\cos(2knz)\, \mathrm{d}z\right], \quad (1)$$

where k is the wave number, $S(k)$ is the spectral intensity distribution of the light source, n is the refractive index, z is the distance measured from the plane where the optical path difference between the reference and sample arms is zero, $a(z)$ denotes the backscattering amplitude of the sample. The first term in Eq. (1) is a constant. The second term is the mutual interference of all elementary waves. The first and second term together give the DC components in the time domain. The third term in Eq. (1) encodes the backscattering amplitude information of the sample. An inverse Fourier transform of the third term in Eq. (1) gives a complex signal $f(z)$, containing amplitude and phase information of the interference signal in time domain. Furthermore, $f(z)$ can be written as

$$f(z) = |f(z)|e^{j\phi(z)}, \quad (2)$$

where $\phi(z)$ is the phasor of $f(z)$.

When there is a moving object passing through the sample volume, there is an equivalent phase front, $\Delta z = nV \cdot k$, adding to z, where n and V are the refractive index of sample and the velocity of the moving object, respectively. The equivalent phase shift will introduce a phase change on $f(z)$, which is the Doppler effect. The corresponding Doppler shift can be estimated by comparing the phasors between two complex signals during two exposures at a same location. Namely, the phase change is recorded by the product of $f_0(z)$ and $f_T*(z)$, where * denotes the conjugate operation and T is the time interval between two exposures and determines the A-line scanning rate. This cal-

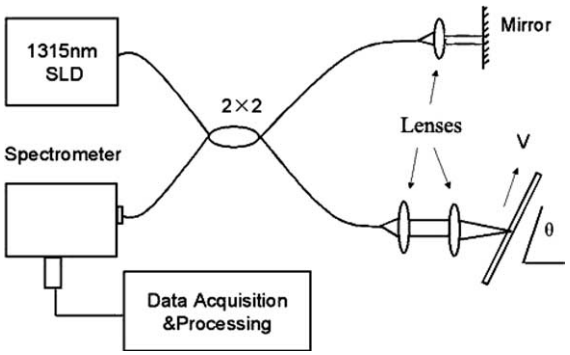

Fig. 1. Phase-resolved frequency domain ODT system. SLD, superluminescent diode; 2×2, fiber coupler; θ, Doppler angle; V, velocity of flow.

culation is integrated for a certain time duration in order to get a better signal-to-noise ratio. The Doppler shift is obtained using the following equation:

$$f_{\mathrm{D}} = \frac{\Delta\phi(z)}{2\pi T} = \frac{\text{argument}\left[\frac{1}{N}\sum_{j=1}^{N}[f_{jT}(z)\cdot f^{*}_{(j+1)T}(z)]\right]}{2\pi T}, \tag{3}$$

where N is the number of A-lines used for averaging. From Eq. (3), two features of phase-resolved ODT can be inferred. First, T determines the Doppler frequency shift range, namely, the velocity dynamic range because $\Delta\phi(z)$ can only be correctly traced between $-\pi$ and π. Second, T determines the imaging speed. Since no mechanical A-line scanning is required in frequency domain, a large velocity dynamical range and an extremely high imaging speed are possible using frequency domain method. Therefore, frequency domain ODT is capable of imaging and quantifying ultra-fast flow dynamics.

In addition to the local velocity information, phase-resolved ODT system gives the variance of local velocity [5], which is given by

$$\sigma^2 = \frac{\int(\omega-\bar{\omega})^2 P(\omega)\,\mathrm{d}\omega}{\int P(\omega)\,\mathrm{d}\omega} = \frac{1}{T^2}\left\{1 - \frac{\left|\frac{1}{N}\sum_{j=1}^{N}\left[f_{jT}(z)\cdot f^{*}_{(j+1)T}(z)\right]\right|}{\frac{1}{N}\sum_{j=1}^{N}\left[f_{jT}(z)\cdot f^{*}_{jT}(z)\right]}\right\}, \tag{4}$$

where $P(\omega)$ is the power spectrum of Doppler frequency shift and $\bar{\omega}$ is the average Doppler frequency shift. The value of σ^2 depends on the flow velocity distribution. Variations of flow velocity broaden the Doppler-frequency spectrum and result in a larger σ^2. Thus, the Doppler variance image obtained by phase-resolved ODT system can be an indicator of flow variations and can be used to study flow turbulences.

Fig. 2 shows the signal-processing flow chart of the phase-resolved frequency domain ODT system. A background light ($F_{\mathrm{b}}(k)$) from reference arm is recorded in advance of data collection. The $F_{\mathrm{b}}(k)$ is subtracted from $F(k)$ in order to reduce the DC component in the time domain. After inversely Fourier transformed, cross-correlation between sequential A-line is calculated. In our experiments, 10 cross-correlations are used for average. Both Doppler shift and variance are calculated from the cross-correlation using Eqs. (3) and (4).

A super-luminescent diode (SLD) with a spectrum centered at 1315 nm and a total delivered power of 8 mW was used. The back-reflected light from the reference arm and the sample arm was dispersed over a 1×512 InGaAs detector array by a 300 mm imaging spectrograph. The total wavelength range spreading on the detector array was 109.7 nm, corresponding to a spectral resolution of 0.21 nm and an imaging depth of 2.2 mm in vacuum. The resulting axial resolution is about 10 μm. The exposure time for each A-line collection was set to 30 μs and the time for data transferring was 530 μs. Thus, the A-line rate we achieved was about 1800 Hz, which gave a velocity dynamic range of 6.0 mm/s at a Doppler angle of 84°. The acquired data were linearized in k space to make the data uniformly sampled. Doppler shift was

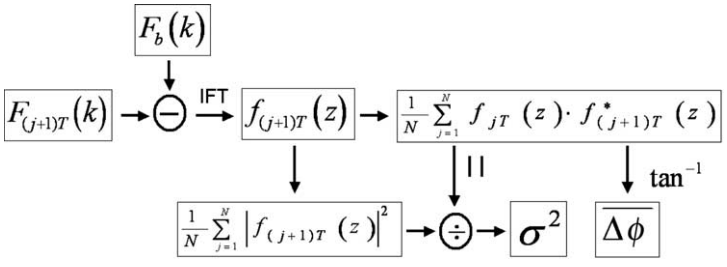

Fig. 2. Computation of phase change and Doppler variance using Eqs. (3) and (4). IFT, inverse Fourier transform; | |, absolute value.

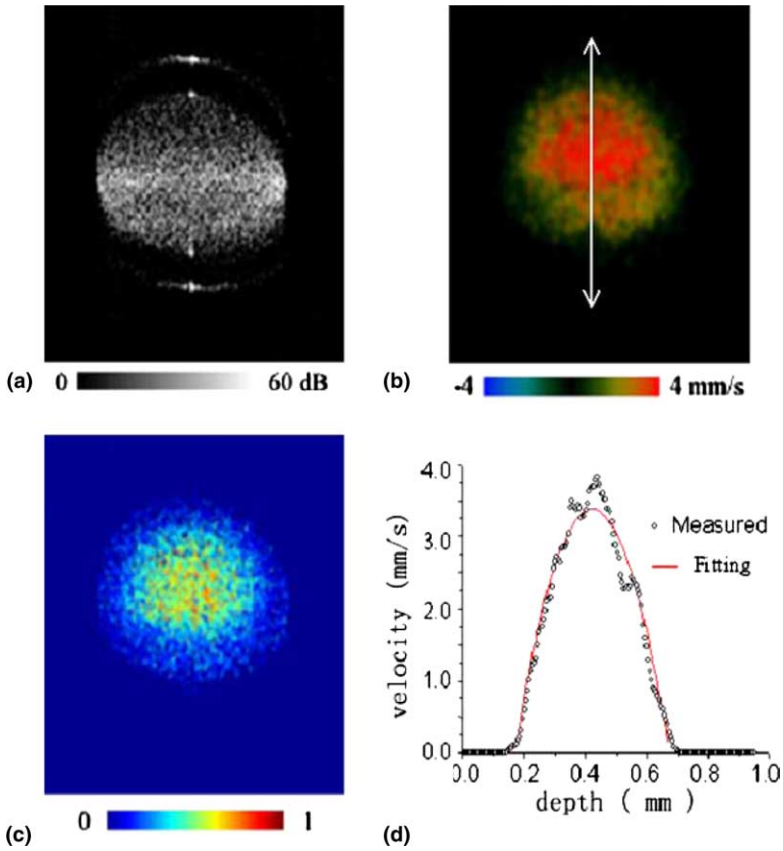

Fig. 3. Structural (a), velocity (b) and normalized Doppler variance (c) images of a fluid flow. (d) Velocity profile along the depth at the center of channel (indicated by an arrowed line in (b)). Circle, measured values; line, parabolic fitting. Image size, 0.75 mm × 0.95 mm; channel dimension, 0.5 mm.

converted to velocity and the Doppler variance was normalized.

Fig. 3 shows the structural, velocity and Doppler variance images of a scattering fluid flowing through a glass channel. The imaging size is 0.75 mm by 0.95 mm. A polystyrene bead solution (mean diameter: 0.3 μm, volume concentration: 0.26%) was used as working fluid. The fluid was driven through a glass channel (outer diameter: 700 μm; inner diameter: 500 μm) by a syringe pump. For this experiment, the fluid was pumped into the glass channel at a rate of 20 μl/min, corresponding to an average flow velocity of 1.70 mm/s within the glass channel. Fig. 3(a) shows the structural image of the glass channel with polystyrene beads. Fig. 3(b) is the velocity image of the flowing fluid. The Doppler angle was set to 86.2°. The velocity was color-coded into red and blue to represent two opposite directions. The presence of different velocities (property of pressure driven flow) within the glass channel was observed. The average velocity measured by the phase-resolved ODT system was 1.66 mm/s. The difference between the measured value and pumped value was within 2.5%. Fig. 3(c) shows the normalized Doppler variance image that gives the variation of the fluid velocity distribution. Fig. 3(d) is the velocity profile along the depth at the center of the channel, indicated by an arrowed line in Fig. 3(b). The profile has a parabolic shape, which reflects the property of pressure-driven flow, as expected.

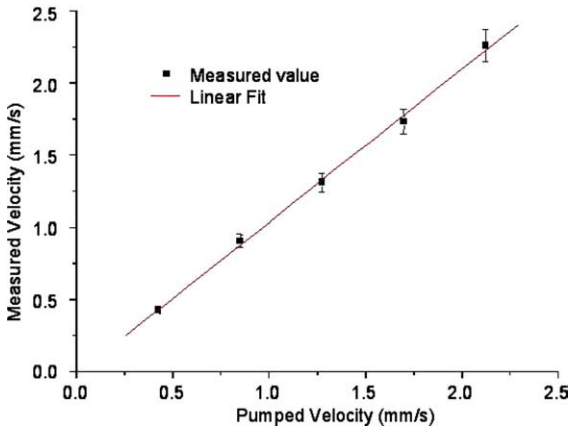

Fig. 4. Measured average velocity vs. pumped average velocity. Solid square, measured values; line, linear fitting. The error bars show 5% error between fitted and measured values.

Flows of the polystyrene bead solution pumped at different velocities were used to test the linearity of the measurement system. The fluid was driven through the same glass channel by a syringe pump. Fig. 4 shows the measured average velocities as a function of pumped average velocities. Solid squares and line denote the measured values and the linear fitting, respectively. The error bar shows 5% error between measured and fitted values. The measured average velocity increased with the increasing of the pumped velocity, as expected.

Fig. 5 shows the structural, velocity and velocity variance images of human finger skin tissues. In Fig. 5, images (a), (c), (e) were taken from the back of a finger, images (b), (d), (f) were taken from the tissue next to the nail. The imaging range was 2.5 mm (width) by 2.2 mm (depth). The structure of finger skin was clearly shown in images (a) and (b). Although the blood vessels were visible ((c) and (d)), Doppler variance images provide a much better mapping of blood vessels ((e) and (f)). The results indicate that it is much easier to identify the blood vessels in the Doppler variance images than in the velocity images. Since the

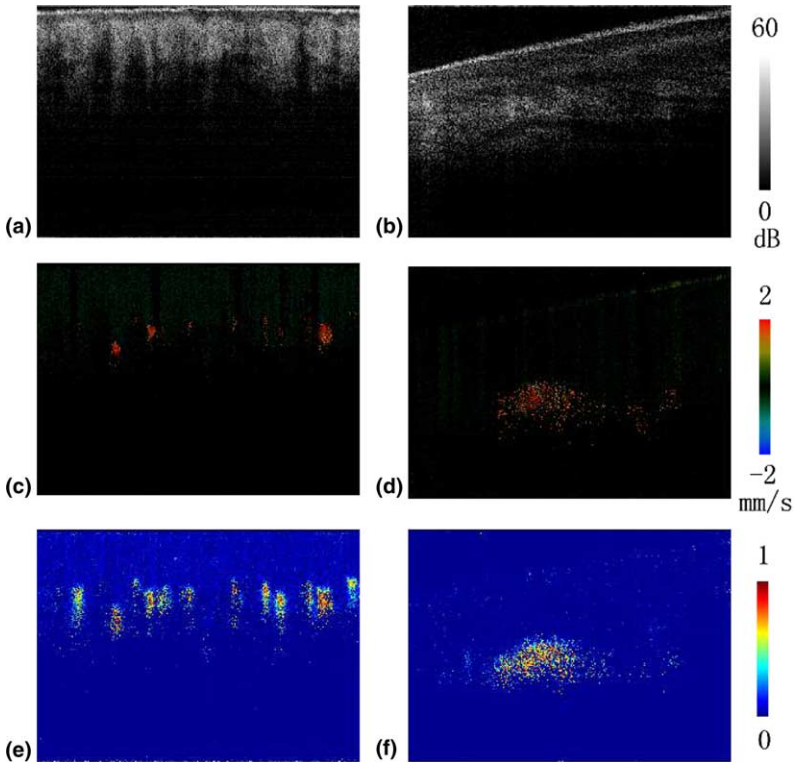

Fig. 5. Doppler and Doppler variance measurements of human finger skin tissues. (a) and (b) structure images of skin tissues; (c) and (d) velocity images of blood flows; (e) and (f) velocity variance images of blood flows. Imaging range, 2.5 mm × 2.2 mm.

orientation of flows buried in non-transparent media cannot be reliably acquired in advance, the Doppler variance images provide a much more accurate mapping of the location of vessels.

As described above, the imaging speed and velocity dynamic range of a phase-resolved ODT system are limited by A-line rate. On the other hand, high A-line rate can also reduce the phase noise caused by environmental vibrations. In frequency domain ODT, no A-scanning is required and only the time between exposures limits the A-line rate. Therefore, the frequency domain method improves the performance of phase-resolved ODT. Ultra-high speed spectrometer with 30 kHz spectral acquisition rates is currently available; if such a high speed spectrometer was used, a frame rate as high as 30 frames/s can be achieved with a velocity dynamic range of 100 mm/s at a Doppler angle of 84°. This would allow for imaging of ultra-fast flow dynamics within complex microfluidic networks, which cannot be accessed by other techniques. In addition, Doppler variance algorithm was also demonstrated to mapping blood vessels in frequency domain. Its advantage for efficiently locating flows buried in non-transparent media was shown.

In summary, we developed a frequency domain phase-resolved ODT system, which incorporated the Doppler variance imaging capability. We used this technique to image fluid flows through microchannel and blood vessels in vivo. This method is capable of achieving much faster imaging speed than the time domain ODT. Given its non-invasive nature, high signal-to-noise ratio, high speed and simple hardware setup, frequency domain phase-resolved ODT is promising for real-time applications, such as imaging and quantifying fast micro-flow dynamics.

Acknowledgments

We acknowledge the support of DARPA Bioflips (N66001-01-C8014), National Science Foundation (BES-86924), National Institutes of Health (EB-00293, NCI-91717) and the Beckman Laser Institute Endowment.

References

[1] Z. Chen, T.E. Milner, D. Dave, J.S. Nelson, Opt. Lett. 22 (1997) 64.
[2] Y. Zhao, Z. Chen, C. Saxer, S. Xiang, J.F. de Boer, J.S. Nelson, Opt. Lett. 25 (2000) 114.
[3] V.X.D. Yang, M.L. Gordon, E.S. Yue, S. Lo, B. Qi, J. Pekar, A. Mok, B.C. Wilson, I.A. Vitkin, Opt. Exp. 11 (2003) 1650.
[4] L. Wang, W. Xu, M. Bachman, G.P. Li, Z. Chen, Opt. Commun. 232 (2004) 25.
[5] Y. Zhao, Z. Chen, C. Saxer, Q. Shen, S. Xiang, J.F. de Boer, J.S. Nelson, Opt. Lett. 25 (2000) 1358.
[6] A.F. Fercher, C.K. Hitzenberger, G. Kamp, S.Y. El-Zaiat, Opt. Commun. 117 (1995) 43.
[7] G. Hausler, M.W. Lindner, J. Biomed. Opt. 3 (1998) 21.
[8] M. Wojtkowski, R. Leitgeb, A. Kowalczyk, A.F. Fercher, In vivo human retinal imaging by Fourier domain optical coherence tomography, J. Biomed. Opt. 7 (2002).
[9] M. Wojtkowski, T. Bajraszewski, P. Targowski, A. Kowalczyk, Opt. Lett. 28 (2003) 1745.
[10] S.H. Yun, G.J. Tearney, J.F. de Boer, N. Iftimia, B.E. Bouma, Opt. Exp. 11 (2003) 2953.
[11] R. Leitgeb, C.K. Hitzenberger, A.F. Fercher, Opt. Exp. 11 (2003) 889.
[12] M.A. Choma, M.V. Sarunic, C. Yang, J.A. Izatt, Opt. Exp. 11 (2003) 2183.
[13] J.F. de Boer, B. Cense, B.H. Park, M.C. Pierce, G.J. Tearner, B.E. Bouma, Opt. Lett. 28 (2003) 2067.
[14] R.A. Leitgeb, L. Schmetterer, C.K. Hitzenberger, A.F. Fercher, F. Berisha, M. Wojtkowski, T. Bajraszewski, Opt. Lett 29 (2004) 171.
[15] L. Wang, Y. Wang, M. Bachman, G.P. Li, Z. Chen, Photonic West 5316 (2004) 432.